JACS
JOURNAL OF THE AMERICAN CHEMICAL SOCIETY
pubs.acs.org/JACS
Article

Sub-Nanometer Mapping of the Interfacial Electric Field Profile Using a Vibrational Stark Shift Ruler

Dhritiman Bhattacharyya, Pablo E. Videla, Joseph M. Palasz, Isaac Tangen, Jinhui Meng, Clifford P. Kubiak,* Victor S. Batista,* and Tianquan Lian*

Cite This: J. Am. Chem. Soc. 2022, 144, 14330−14338
Read Online
ACCESS | Metrics & More | Article Recommendations | Supporting Information

ABSTRACT: The characterization of electrical double layers is important since the interfacial electric field and electrolyte environment directly affect the reaction mechanisms and catalytic rates of electrochemical processes. In this work, we introduce a spectroscopic method based on a Stark shift ruler that enables mapping the electric field strength across the electric double layer of electrode/electrolyte interfaces. We use the tungsten-pentacarbonyl(1,4-phenelenediisocyanide) complex attached to the gold surface as a molecular ruler. The carbonyl (CO) and isocyanide (NC) groups of the self-assembled monolayer (SAM) provide multiple vibrational reporters situated at different distances from the electrode. Measurements of Stark shifts under operando electrochemical conditions and direct comparisons to density functional theory (DFT) simulations reveal distance-dependent electric field strength from the electrode surface. This electric field profile can be described by the Gouy−Chapman−Stern model with Stern layer thickness of ∼4.5 Å, indicating substantial solvent and electrolyte penetration within the SAM. Significant electro-induction effect is observed on the W center that is ∼1.2 nm away from the surface despite rapid decay of the electric field (∼90%) within 1 nm. The applied methodology and reported findings should be particularly valuable for the characterization of a wide range of microenvironments surrounding molecular electrocatalysts at electrode interfaces and the positioning of electrocatalysts at specific distances from the electrode surface for optimal functionality.

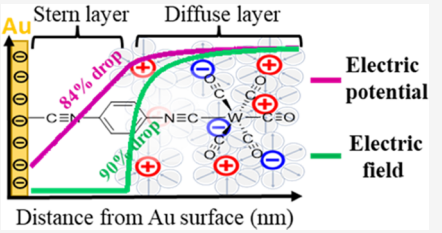

INTRODUCTION

Understanding and characterizing the nature of electric fields surrounding catalytic centers at electrode/electrolyte interfaces, or confined in molecular microenvironments, is an outstanding challenge of great current interest. The voltage applied in a typical electrochemical experiment generates an interfacial electrostatic potential that is rapidly screened by the dielectric solvent and the supporting electrolyte in the electric double layer (EDL), giving rise to large interfacial electric fields on the order of 1 V/nm at the electrode/electrolyte interface.[1,2] Surface-bound molecules feel the effect of the interfacial field and can drastically change their behavior, even to the extent of changing their chemical reactivity as influenced by the applied bias potential.[1,3−11] However, the characterization of the interfacial electric field remains challenging. Here, we introduce a spectroscopic method based on a molecular Stark shift ruler that enables mapping of the electric field strength across the electric double layer of electrode/electrolyte interfaces.

Theoretical models such as the Gouy−Chapman−Stern (GCS) model,[12−14] later modified by Bockris et al.,[15] is commonly used for the analysis and interpretation of EDL. According to GCS model, EDL consists of a Stern layer and a diffuse layer; and the electric potential, as a function of distance from the electrode surface, first drops linearly within the Stern layer and exponentially in the diffuse layer. Experimental characterization of the EDL structure is important as it directly influences the electric potential distribution within these layers and, therefore, affects the reaction mechanisms and rates of various electrochemical processes. Electrochemical impedance spectroscopy, differential capacitance, or surface tension measurements are conventionally used to probe the structure of EDL. These techniques report macroscopic quantities, such as capacitance or current−voltage plots, which obfuscate discrete molecular behavior at the interface. As a result, processes like ion-paring in the double layer, specific adsorption, and strong nonspecific interaction of ions with the electrode (ion condensation)[16] that severely affect the electrolyte distribution and hence the electric field profile inside the EDL (typically on the nanometer scale), cannot be directly probed using these techniques. On the other hand, vibrational Stark shift spectroscopy[17−20] allows us to directly measure the electric fields experienced by the molecules at the electrochemical interface and explore how nuanced changes in the electro-

Received: May 25, 2022
Published: July 29, 2022

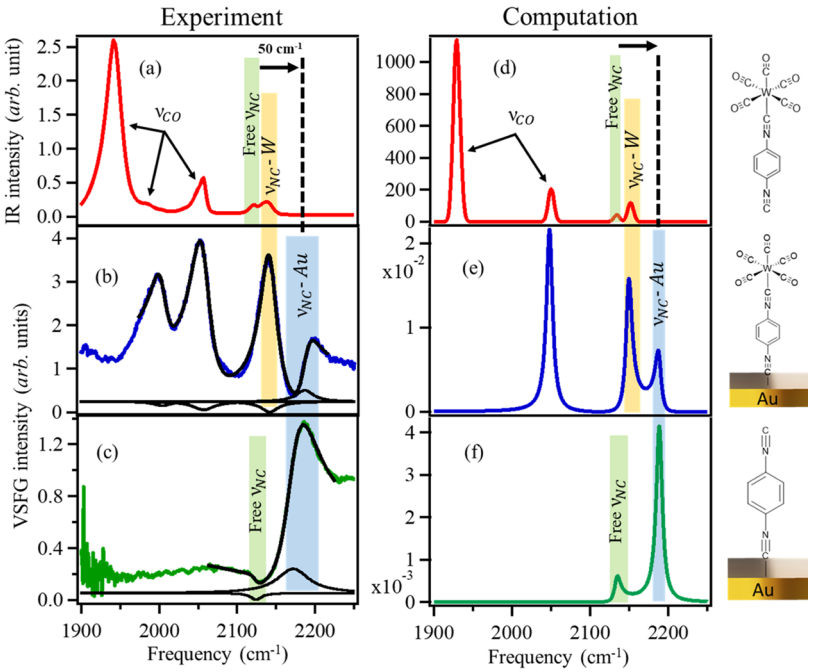

Figure 1. (a) Experimental and (d) computed IR spectrum of PDI-$W(CO)_5$ in DCM. A representative PPP-VSFG spectrum (blue) of PDI-$W(CO)_5$ SAM on the Au surface: (b) experiment, measured at -0.4 V vs Ag/Ag^+ reference electrode, and (e) computation. The fit of the experimental spectrum is shown in black.[52] PPP-VSFG spectrum (green) of PDI SAM on the Au surface: (c) experiment and (f) computation. The fit is shown in black. A cartoon drawing of each molecular system is shown on the right of the respective figure. The green, yellow, and sky-blue-colored vertical lines represent the frequencies of the free NC group, NC−W, and NC−Au, respectively. Four Lorentzians were used to fit the experimental spectrum in Figure 1b, whereas two Lorentzians were used to fit the spectrum in Figure 1c (see the SI). The imaginary part of each Lorentzian used in this fitting exercise is shown underneath the experimental spectrum.

chemical conditions modulate the interfacial environment at a molecular scale.[21−27]

A great volume of in situ electrochemical Stark shift studies that involve operando infrared (IR), Raman, and interface-specific vibrational sum frequency generation (VSFG) spectroscopies has been dedicated to elucidating the structure of EDL.[23,24,28−30] Early works were focused on measuring Stark tuning rates of small, prototypical species (molecules or ions) such as CO, CN^-, and SCN^- adsorbed on coinage metal surfaces, giving an estimation of the interfacial electric field within ∼1−3 Å from the electrode surface.[22,25,31−39] Larger molecular probes have also been investigated; for example, in the case of nitrile-terminated self-assembled monolayers (SAMs) or our own work on group VII metal carbonyl complexes, the Stark shift reporter (CN or CO) probes electric field strength at a single spatial position away from the electrode surface (3−6 Å);[24,40] and, therefore, cannot measure the decay of electric potential as a function of distance from the electrode, by construct. Using the method proposed by Smith and White[41] and later extended by Fawcett,[42] Eggers et al.[43] calculated the potential drop within EDL by measuring the effect of electric field on the formal potential of a series of ferrocene-terminated norbornylogous bridges, where the redox active ferrocene moiety was placed at fixed distances from the electrode surface. Most recently, Wen et al.[44] used a series of seven viologen SAMs on an Au (111) surface, with the 4,4′-bipyridinium Raman marker located at different distances from the electrode. By monitoring the change in resonant Raman intensity between different SAMs, they were able to measure the change in electric field distribution within the EDL. While these results were scientifically illuminating and encouraging, one must remember that the interfacial environments of different SAMs are not identical; the molecular packings are different, which dictates the extent of electrolyte penetration within the SAM, affecting the potential of zero charge (PZC) and the structure of the EDL, in general.

An ideal molecular system to map out the electric field distribution in the double layer is one that has multiple localized vibrational markers present at different positions on the same molecule. For example, 1,4-phenylenediisocyanide (PDI) forms a SAM on gold surfaces with one of the NC groups bound to Au while the other NC group is free, i.e., a system with two Stark reporters at two different distances from the metal electrode. Surface-enhanced Raman spectroscopy (SERS) measurement of PDI SAM on gold shows a large response for the NC bound to Au, whereas that of the free NC group is weak and buried under the much stronger bound NC peak, making it difficult to determine its frequency accurately.[45] Our recent endeavor to measure the VSFG spectrum of PDI SAM on gold produces a similar result.[46] In the present work, we show that the VSFG response of this weak NC group of PDI can be greatly enhanced by synthetically attaching it to -$W(CO)_5$, allowing one to clearly identify the corresponding peak position. The choice of this transition metal complex is deliberate, as group VI metal carbonyls are well-known for their ability toward catalytic CO_2 reduction,[47] which makes PDI-$W(CO)_5$ molecular system an ideal mimic for attached molecular electrocatalysts.[48,49] Moreover, the PDI-$W(CO)_5$ SAM on gold presents us with multiple Stark reporters (Au-bound NC group, W-bound NC group, axial and equatorial CO of $W(CO)_5$) within a single molecular system but located at different spatial distances from Au electrode. Stark shift measurement of these vibrational modes under electrochemical conditions has allowed us to map

https://doi.org/10.1021/jacs.2c05563
J. Am. Chem. Soc. 2022, 144, 14330−14338

out the strength of the electric field at multiple points within the EDL, presenting the first experimental evidence of its kind to quantitatively establish the drop of electric potential within the double layer.

The complex PDI-$W(CO)_5$ was previously synthesized and characterized in great detail.[50] The Fourier transform infrared (FTIR) spectrum of PDI-$W(CO)_5$ complex dissolved in anhydrous dichloromethane (DCM) is shown in Figure 1a. The computed IR spectrum of this complex is shown in Figure 1d. There are two peaks in the region between 2100 and 2200 cm^{-1}, corresponding to the NC bound to W appearing at ~2146 cm^{-1} (shaded yellow) and the free NC group at ~2127 cm^{-1} (shaded green). The other three peaks at ~2060, ~2000, and ~1950 cm^{-1} correspond to three CO stretching modes of the -$W(CO)_5$ moiety. As previously shown by Burdett et al.[51] and also confirmed by our own theoretical calculation (see the Supporting Information), the ~2000 cm^{-1} mode should be IR inactive; yet, this mode appears in the solution IR spectrum of PDI-$W(CO)_5$ (albeit very weak in intensity). This can be attributed to a Fermi resonance resulting from its interaction with the overtone transition ($\nu = 0 \rightarrow \nu = 2$) of the IR-active C−H in-plane bending mode of the PDI molecule, which has a fundamental frequency of ~1012 cm^{-1}.[45] Fermi resonance originates from vibrational anharmonicity in a molecular system, and therefore our theoretical calculation, performed under harmonic approximation, could not predict the occurrence of this mode.

A representative PPP-polarized VSFG spectrum of the SAM of PDI-$W(CO)_5$ complex on the planar polycrystalline gold surface is shown in Figure 1b. The computed PPP-VSFG spectrum is shown in Figure 1e. The details of the experiment and computation can be found in the Supporting Information. The free NC group (as shown in Figure 1a,d) binds to the Au surface, donating its carbon-centered σ-lone pair of electrons without π-backbonding (Au is an s-band metal) and thus is blue-shifted by ~50 cm^{-1}, consistent with previous IR, SERS, and VSFG studies.[46,53−58] The selection rule of VSFG spectroscopy dictates that for a vibrational mode to be VSFG active, it must be both IR- and Raman-active.[59] To find the Raman-active modes of the molecule, we measured shell-isolated nanoparticle-enhanced Raman (SHINER)[28] spectrum of PDI-$W(CO)_5$ SAM attached to a planar Au surface (Figure S3), which shows three prominent peaks corresponding to Au-bound NC, W-bound NC, and W-bound CO vibrational modes. Our theoretical calculation also corroborates this result, which predicts the ~2175, ~2145, and ~2060 cm^{-1} modes to be both IR- and Raman-active (Figure S7), and therefore, we find three prominent peaks at respective frequencies in the experimental VSFG spectrum, as expected from the selection rule. The ~1950 cm^{-1} mode shows considerable intensity in the solution IR spectrum, as also predicted by our calculation (Figure 1). However, this mode is not observed in the experimental SHINER spectrum (Figure S3), and the theoretically calculated Raman intensity of this mode is also negligible as compared to other vibrations (Figure S7). As a result, the ~1950 cm^{-1} band is absent in the PPP-polarized VSFG spectrum. Figure 1b also shows a prominent peak at ~2000 cm^{-1}, attributed to the Fermi resonance discussed above. Observation of such a Fermi-resonance transition in VSFG is not unprecedented and is consistent with previous literature reports on other systems.[60] To extract frequencies of different vibrational modes of the surface-bound PDI-$W(CO)_5$ molecules, the VSFG spectrum is fitted using eq (1) mentioned in the Supporting Information. Each resonant mode is modeled using a Lorentzian; the imaginary part of each Lorentzian is shown underneath the VSFG spectrum.

We also measured the PPP-VSFG spectrum of a PDI SAM on the Au surface (Figure 1c). The computed spectrum is shown in Figure 1f. As evident from the experiment, the NC group bound to gold shows a strong response, whereas the VSFG intensity of the free NC group is much weaker, making it hard to identify the corresponding peak position. Attaching the -$W(CO)_5$ moiety to this free NC group enhances the VSFG intensity of this mode by ~25×, as predicted by our calculation (contrast Figure 1e,f). Such enhancement manifests itself in our experimental VSFG spectrum (Figure 1b), with a clear peak corresponding to NC attached to W at ~2145 cm^{-1}. Moreover, such chemical modification presents us with a new molecular system with an additional vibrational reporter (CO attached to W) at an even further distance from the gold surface, allowing us to measure the electric field strength well beyond 1 nm from the electrode.

Electrochemical Stark Shift of PDI-$W(CO)_5$ SAM at Au/Liquid Interface. The potential-dependent VSFG spectra of PDI-$W(CO)_5$ adsorbed on Au is shown in Figure 2a. All

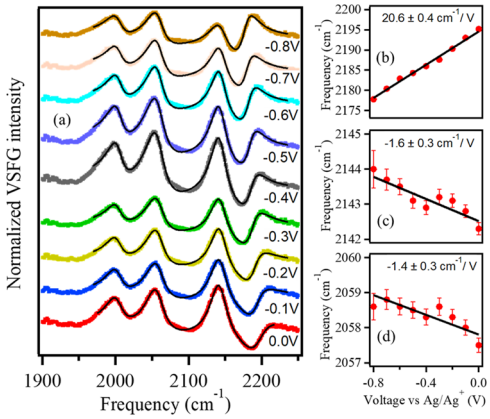

Figure 2. (a) Normalized PPP-VSFG spectra measured under in situ electrochemical conditions at nine different electrode potentials (vs Ag/Ag^+). A 0.2 M tetrabutylammonium hexafluorophosphate ($TBAPF_6$) in dichloromethane (DCM) is used as the electrolyte solution. The SAM-decorated Au slide and a Pt wire were used as working and counter electrodes, respectively. Vibrational frequency of each mode was extracted by spectral fitting procedure, as described in the Supporting Information, and plotted as a function of electrode potential: (b) NC bound to Au, (c) NC bound to W, and (d) CO bound to W.

spectra were fitted to extract the frequencies of different vibrational modes of the surface-bound PDI-$W(CO)_5$ molecules. The center frequency of each vibration was extracted (shown in Table S4) and plotted as a function of potential (vs Ag/Ag^+), shown in Figure 2b−d. The shift of the Fermi-resonance mode frequency is not shown, as we will not be using it for the calculation of interfacial electric field. The frequency vs potential plot for each vibrational mode can be fitted with a linear equation, with the fitted line representing the slope of the Stark shift in cm^{-1}/v unit. The slopes of NC bound to Au (Figure 2b) and NC bound to W (Figure 2c) are of opposite sign, as expected from the opposite direction of these two NC dipole moments.[46] Upon applying external bias, the generated electric field is assumed to be in the direction perpendicular to the electrode surface. One of these NC

https://doi.org/10.1021/jacs.2c05563
J. Am. Chem. Soc. 2022, 144, 14330−14338

dipoles, which is aligned to this electric field, becomes stabilized, while the other dipole moment vector, opposing the electric field, gets destabilized, thereby showing opposite signs of the Stark shift slopes. The magnitude of the slopes carries information about the strength of the local electric field experienced by the vibrational probe.

Calculating the Interfacial Electric Field as a Function of Potential. We correlate this interfacial electric field to the potential-dependent frequency of the vibrational probes as follows:

$$\omega(\varphi) = \omega_0 + \overrightarrow{\Delta\mu}.\vec{F}(\varphi) \quad (1)$$

where, $\vec{F}(\varphi)$ is bias-dependent electric field strength, ω_0 and $\omega(\varphi)$ stand for the vibrational frequencies in the absence of applied voltage and at potential φ, respectively. $\overrightarrow{\Delta\mu}$ is known as the Stark tuning rate, representing the susceptibility of a vibrational probe toward applied electric field. We remark that $\overrightarrow{\Delta\mu}$ is related to the change in vibrational transition dipole and for a localized vibration on a bond or small functional group reports on the local electric field projected along the mode.[17−19,61] To determine $\overrightarrow{\Delta\mu}$, we performed density functional theory (DFT) frequency calculations for PDI-$W(CO)_5$ molecule attached to Au cluster, with an external uniform electric field ranging from −1 to +1 V/nm applied perpendicular to the surface (Figure 3c). Figure 3a shows the simulated vibrational spectra of PDI-$W(CO)_5$ attached to Au (see the SI for details) as a function of the applied field. The frequency of each vibrational mode is plotted with respect to an electric field, and the slope of this plot determines $\Delta\mu$, as shown in Figure 3b, for three vibrational modes: NC−Au (red), NC−W (blue), and CO−W (green). It is to be noted that the calculated $\Delta\mu$ for NC−Au and NC−W vibrational modes have opposite signs, consistent with experimental observation.

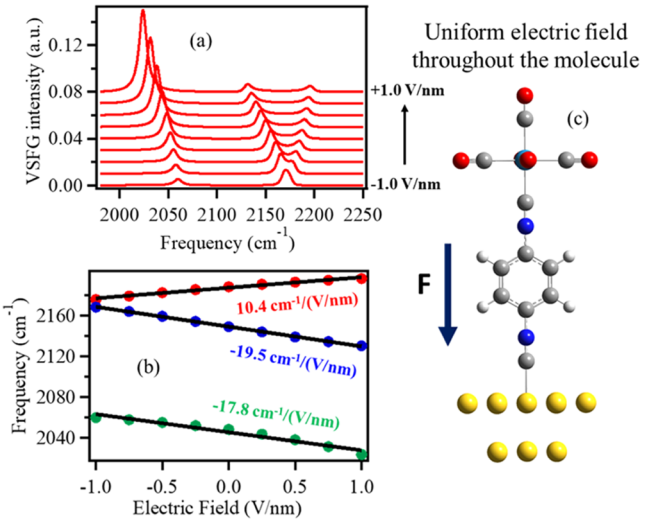

Figure 3. (a) Computed PPP-VSFG spectra as a function of the external electric field between −1 and +1 V/nm. (b) Theoretically calculated frequency of each vibrational mode is plotted with respect to an electric field, and the slope of this plot determines $\Delta\mu$ (in cm^{-1}/(V/nm) unit): NC−Au (red), NC−W (blue), and CO−W (green). (c) Cartoon figure representing PDI-$W(CO)_5$ molecule attached to Au cluster, with an electric field applied perpendicular to the surface.

Table 1 above represents the experimental Stark Slope and the calculated $\Delta\mu$ values for Au attached PDI-$W(CO)_5$ molecules, as compared to our previously published results on Au-PDI system. The large values of calculated $\Delta\mu$ for all of the vibrational modes of PDI-$W(CO)_5$ on Au deserve a special mention. As shown in Table 1, the value of $\Delta\mu$ for the free NC group of PDI adsorbed on Au is −5.3 cm^{-1}/(V/nm); whereas in case of PDI-$W(CO)_5$ on Au, the $\Delta\mu$ value of the NC group attached to W is −19.5 cm^{-1}/(V/nm). Therefore, attachment of -$W(CO)_5$ moiety to the free NC group increases its $\Delta\mu$ value by about 4 times. This can be understood as follows: tungsten (W) is a 5d transition metal and is highly polarizable. Attaching an NC group to W is achieved via σ-donation of a C-centered electron pair to the empty d orbitals of the metal center, followed by significant backdonation of electron density from the W dπ orbitals to the π^* orbital of the NC species via dπ−pπ interaction. This increases charge separation within N≡C−W species, making it more susceptible toward the external electric field. We also believe that the higher polarizability of this N≡C−W coupled vibration is responsible for the enhancement (∼25 times) of its VSFG signal intensity (Figure 1), as compared to that of the free NC group in Au-bound PDI molecule. The calculated $\Delta\mu$ values for Au-bound NC and W-bound CO groups also appear to be equally strong. In all of these cases, the common factor is a 5d transition metal (either Au or W), where each vibrational probe is localized. Therefore, we conclude that attachment of a highly polarizable metal center to a vibrational probe, which otherwise has a small $\Delta\mu$ value, can be used as a chemical tool to drastically enhance its susceptibility toward the applied electric field. A large $\Delta\mu$ value of a vibration makes it easier to experimentally measure its frequency shift under applied bias, especially in the region where the electric field strength is very low. For example, given the electrolyte concentration used in our experiment (0.2 M), the electric potential is expected to drop almost entirely within 1 nm distance from the electrode surface. Despite that, large $\Delta\mu$ values of different vibrational probes of the PDI-$W(CO)_5$ system have allowed us to measure the electric field strength well beyond 1 nm from the Au surface, which would otherwise be very challenging to measure.

Starting with eq 1, the expression of the absolute electric field strength as a function of applied voltage ($F(\varphi)$) can be deduced as shown in the Supporting information.

$$F(\varphi) = \frac{d\omega(\varphi)}{d\varphi}.\frac{1}{\Delta\mu}.(\varphi - \varphi_{PZC}) \quad (2)$$

$\frac{d\omega(\varphi)}{d\varphi}$ is measured experimentally, while $\Delta\mu$ is calculated theoretically. φ_{PZC} represents the potential of zero charge (PZC) of the Au/SAM/electrolyte system. Based on literature reports of various Au/electrolyte systems[62−65] and our previous work on PDI,[46] we assume the PZC for Au/PDI-$W(CO)_5$/electrolyte system to be ∼ −0.05 V vs Ag/Ag^+, which enables us to calculate the strength of the interfacial electric field. The calculated absolute electric field strength ($F(\varphi)$) observed by all three vibrational modes as a function of applied voltage (φ) is shown in Figure 4a, and the slope $\left(\frac{dF(\varphi)}{d\varphi}\right)$ is tabulated in Table 1. We should stress that this calculated electric field does not depend on any specific double-layer model. However, we remark that an assumption underlying the use of eq 2 is that the value of $\Delta\mu$ obtained for the vibrational probe under a uniform external electric field

https://doi.org/10.1021/jacs.2c05563
J. Am. Chem. Soc. 2022, 144, 14330−14338

Table 1. Comparison of L, $\frac{d\omega(\varphi)}{d\varphi}$, $\Delta\mu$, $\frac{dF(\varphi)}{d\varphi}$ of PDI, and PDI-W(CO)$_5$ SAMs on Au

SAM/Au	L (Å)	$\frac{d\omega(\varphi)}{d\varphi}$ (cm^{-1}/V)			$\Delta\mu$ (cm^{-1}/(V/nm))			$\frac{dF(\varphi)}{d\varphi}$ (nm^{-1})		
		NC−Au	free NC		NC−Au	free NC		NC−Au	free NC	
PDI[a]	9.8	16 ± 4	1 ± 3		10.3	−5.3		0.9 ± 0.3		
PDI-W(CO)$_5$	15.3	NC−Au	NC−W	CO−W	NC−Au	NC−W	CO−W	NC−Au	NC−W	CO−W
		20.6 ± 0.4	−1.6 ± 0.3	−1.4 ± 0.3	10.4 ± 0.5	−19.5 ± 0.2	−17.8 ± 1.4	1.98 ± 0.04	0.08 ± 0.01	0.08 ± 0.01

[a]Results for PDI SAM on Au are taken from our previous publication.[46] 'L' is the estimated thickness of the SAM (DFT molecular length + C−Au bond). $\frac{d\omega(\varphi)}{d\varphi}$ is measured experimentally and represents the slope of the change in frequency as a function of applied voltage, while $\Delta\mu$ is calculated using DFT. $\frac{dF(\varphi)}{d\varphi}$ represents the slope of electric field vs voltage plot (Figure 4a).

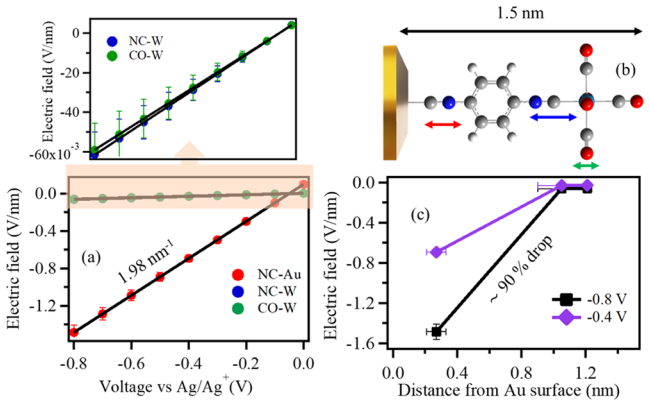

Figure 4. (a) Calculated electric field experienced by different vibrational modes: NC−Au (red), NC−W (blue), and CO−W (green) as a function of applied voltage. The blue and green plots are shown on the top in a zoomed-in view. The slopes of these plots are mentioned in Table 1. (b) PDI-W(CO)$_5$ molecule on the Au surface. The DFT-calculated length of the molecule is 1.5 nm. The red, blue, and green arrows represent the spatial extent of NC−Au, NC−W, and CO−W vibrational modes, respectively. (c) Calculated electric field strength for two different voltages (−0.8 V, black and −0.4 V, purple) as a function of distance from the electrode surface.

remains unchanged even if the whole molecule is subject to a nonuniform, spatial-dependent field. We are currently working toward the development of a more rigorous calculation, where the Stark shift is computed assuming a distance-dependent field distribution that the molecules experience in the double layer and iteratively modify that field profile until it reproduces the experimentally measured frequencies. We believe such an approach will be proven useful for conjugated (highly polarizable) molecules, where the Stark tuning rate of a functional group may depend on the field strength that the rest of the molecule experiences. On the contrary, for non-conjugated weakly polarizable molecules, this would likely not yield a major difference.

Electric Field Strength as a Function of Distance From the Au Surface. One important parameter to map out the electric field strength within the electrochemical double layer is the spatial location of each vibration of the SAM with respect to the electrode surface. Our normal mode analysis of PDI-W(CO)$_5$ system on Au (111) cluster reveals that each vibrational mode measured by VSFG is fairly localized, providing us with vibrational probes of the local field at a sub-molecular scale (see the SI). As evident from Table S1 in the Supporting information, the 2188 cm^{-1} mode is entirely localized to the NC stretching vibration attached to Au (~99%). The ~2149 and ~2048 cm^{-1} modes are somewhat mixed, but the former has a predominant contribution from N≡C−W coupled vibration, whereas the latter is mostly localized on W-bound equatorial carbonyl groups. Thus, considering the estimated thickness of the SAM (~1.5 nm), these three vibrational modes (N≡C−Au, N≡C−W, and CO$_{equiv}$−W) are localized approximately at 2.7 ± 0.6, 10.5 ± 1.0, and 12.5 ± 0.0 Å, respectively, from the Au surface, as shown by red, blue, and green arrows in Figure 4b. This allows us to measure the strength of the local electric field with Angstrom spatial resolution and to map out how, in a typical SAM-modified-metal/electrolyte interface (analogous to the heterogeneous electrocatalytic system with a monolayer of catalyst attached to the electrode), the electric field decays as a function of distance from the electrode surface. As evident from Figure 4c, there is a precipitous drop (~90%) in the strength of the electric field within 1 nm from the electrode surface, and beyond that, the decay is much more gradual. We should emphasize that measuring such a small electric field at >1 nm distance from the electrode surface has only become possible because of the large $\Delta\mu$ values of the vibrational probes of PDI-W(CO)$_5$ molecular system.

Comparing Our Result with Existing Double-Layer Models. Gouy−Chapman (GC) and Gouy−Chapman−Stern (GCS) models are two of the widely invoked theories that are used to explain double-layer structure at an electrode−electrolyte interface. The classic GC model considers a diffuse layer near the electrode, and the electric field is assumed to drop exponentially as a function of distance from the electrode surface and decreases to the $1/e$ of its maximum value at the Debye length, which is estimated to be ~0.23 nm for a 0.2 M solution of TBAPF$_6$ in DCM (ε = 8.93) and at room temperature (T = 293 K). On the other hand, the GCS model assumes a Stern layer and a diffuse layer in the double-layer structure; the electric potential drops linearly within the Stern layer, and in the diffuse layer, it drops exponentially. Electric field is the negative gradient of potential; therefore, a linear drop of potential within the Stern layer results in a constant electric field in this region. Now, we want to explore how effective these double-layer models are into reproducing our experimental findings. Detailed descriptions and important equations related to these models are mentioned in the Supporting information.

Figure 5 compares our experimental results with GC and GCS models. The black circles in Figure 5b represent our experimentally determined electric field at −0.8 V vs Ag/Ag$^+$. The GC model (black dotted line) consistently underestimates the electric field strength by ~90−95% compared to our experiment. Such a result is not unprecedented, as this model does not consider SAM formation on the electrode surface and

https://doi.org/10.1021/jacs.2c05563
J. Am. Chem. Soc. 2022, 144, 14330−14338

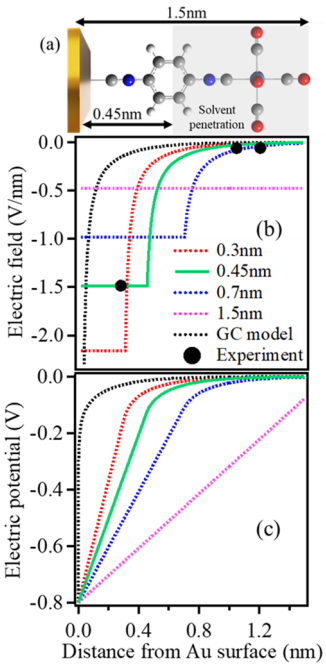

Figure 5. (a) Cartoon picture of PDI-$W(CO)_5$ molecule on Au, showing the solvent penetration within SAM and the effective thickness of the Stern layer (0.45 nm). (b) Electric field (at −0.8 V vs Ag/Ag^+) as a function of distance from the electrode surface: this work (black circles), simulation based on GC model (black dotted line), and for different thicknesses of the Stern layer (x_2), 0.3 nm (red), 0.7 nm (blue), 1.5 nm (pink), and 0.45 nm (solid green). As evident from this plot, simulation with x_2 = 0.45 nm satisfactorily reproduces our experimental observation. (c) Simulated electric potential as a function of distance from the Au surface. For x_2 = 0.45 nm, the electric potential drops linearly by ∼83% within the Stern layer, and beyond that, the potential drops exponentially in the diffuse layer.

therefore is far from experimental reality. This result, however, highlights the importance of the surface-attached molecules that play a significant role to alter the double-layer structure at an electrode/electrolyte interface. On the other hand, the GCS model does consider a Stern layer (which can be approximated as the SAM) and is better suited to mimic our experiment. We first assume the extreme scenario where the length of the Stern layer is equal to the length of the SAM, i.e., 1.5 nm, and the simulated electric field in this case shows a constant value throughout as a function of distance from the electrode surface (pink dotted line), and therefore, is unable to predict the drop in electric field strength within the SAM, as observed experimentally. This points to the fact that the effective thickness of the Stern layer (x_2) is smaller than that of the SAM itself, possibly due to solvent and electrolyte penetration within SAM.[46,66] To find the value of x_2, we have simulated the electric field profile within the double layer as a function of different extent of solvent penetration within SAM, and for x_2 = 0.45 nm, the simulation (solid green line) satisfactorily reproduces our experimental electric field strength. The simulated electric fields for x_2 = 0.3 nm (dotted red line) and x_2 = 0.7 nm (dotted blue line) are also shown in the same plot to demonstrate that the interfacial field profile is hugely dependent on the extent of solvent penetration within the SAM. We believe that the bulky nature of the -$W(CO)_5$ moiety prevents the formation of a densely packed SAM on the gold surface, leaving enough room for the solvent and the electrolyte to penetrate, which makes the effective thickness of the Stern layer to be ∼4.5 Å; beyond that, it is just like a Gouy−Chapman diffuse layer (Figure 5a). In Figure 5c, we have also plotted the electric potential as a function of distance from the electrode surface using simulations based on GC model and for different thicknesses of the Stern layer. For x_2 = 0.45 nm (solid green line), we estimate that there is a linear potential drop ($\Delta\varphi = \varphi_2 - \varphi_0$) by ∼83% within the Stern layer and an exponential drop further away from the electrode.[67,68] On the contrary, in the scenario of no solvent penetration within SAM, i.e., for x_2 = 1.5 nm, the electric potential decays much slowly, and therefore, the same ∼83% drop would take place over a distance of 1.4 nm from the Au surface (Figure 5c, pink line). Our experiment, along with simulation, demonstrates that the precipitous drop in electric field happens while moving across from the effective Stern layer to the diffuse layer. This result will be an invaluable design consideration in heterogeneous electrocatalysts, where the catalytic center should be constrained to be within half a nanometer from the electrode surface for optimal field-induced performance. From an experimental perspective, the extent of solvent penetration within the SAM can be controlled by changing the size of the cation and anion in an electrolyte solution. Moreover, changing the solvent (i.e., change in dielectric constant) will also change the extent of screening of the electric potential and thereby change the electric field profile in the double layer. A detailed study to unravel these effects is underway.

CONCLUSIONS

We have combined in situ vibrational sum frequency generation (VSFG) spectroscopic measurements and DFT calculations of VSFG spectra to probe the electric field across the double-layer structure in a typical electrode/SAM/electrolyte interface. The PDI-$W(CO)_5$ SAM on the Au surface serves as a mimic for heterogeneous electrocatalysis, since group VI metal carbonyls are well-known for their ability toward catalytic CO_2 reduction. The PDI-$W(CO)_5$ system has multiple Stark reporters situated at different distances from the electrode surface, allowing us to measure the local electric field with sub-Å spatial resolution. Our results show that there is a precipitous drop (∼90%) in electric field strength within 1 nm from the Au surface and a more gradual further drop farther away from the surface. We emphasize that our work uses a single Au/SAM system and is different from previous attempts that employ a series of SAMs of different lengths. Changing the molecular length changes the packing density of the SAM, which controls the extent of electrolyte penetration within the Stern layer, affecting the potential of zero charge (PZC) and the structure of the EDL, in general. Our work does not suffer from these issues and, therefore, is the first attempt of its kind to map out the electric field strength up to 1.3 nm from the electrode surface. Moreover, the large value of the Stark tuning rates ($\Delta\mu$) for all vibrational probes in the PDI-$W(CO)_5$ system allows us to probe a very weak electric field far away from the electrode (>1 nm), which would otherwise be difficult to measure with conventional Stark reporters with $\Delta\mu$ values 4−5 times smaller than in our case.

We have shown that the prediction of GC model is far from our experimental findings, quite understandably. Under the realm of GCS model, considering the length of the Stern layer to be equal to that of the SAM also fails to reproduce the experiment. Therefore, we have adopted a more realistic

https://doi.org/10.1021/jacs.2c05563
J. Am. Chem. Soc. 2022, 144, 14330−14338

double-layer model by explicitly considering solvent and electrolyte penetration within the SAM. Our simulation of the electric field predicts the effective thickness of the Helmholtz layer to be ∼4.5 Å; beyond that, it looks just like a Gouy−Chapman diffuse layer; and it is the juncture between these two layers, where the majority drop (∼90%) in the electric field takes place. The electric potential linearly drops by ∼83% within the Helmholtz layer itself. We should emphasize that our work focuses on characterizing the interfacial double-layer structure of a SAM-modified electrode surface (that obviously differs from the one without the SAM) and mimics the EDL structure of a heterogeneous electrocatalysis process, where the interface is decorated with a layer of molecular catalyst. Therefore, the reported conclusions should be carefully considered when designing a molecular electrocatalyst, where positioning of the catalytic center at a particular distance from the electrode surface is of pivotal importance. Catalytic centers at chiral microenvironments could also be selectively probed analogously, using chiral SFG methods.[69,70] Future works from our groups will focus on varying different parameters, including the surface coverage of the SAM, the size of the cations and anions in the electrolyte, and its ionic strength to systematically control the interfacial environment and its effect on the electric field profile across the double layer. Moreover, from the theoretical point of view, we will design spatial-dependent electric field profiles to investigate the Stark effect susceptibility of localized vibrational probes to nonuniform fields. That level of characterization will provide a realistic model of the double-layer structure for universal adoption.

■ ASSOCIATED CONTENT

Supporting Information

The Supporting Information is available free of charge at https://pubs.acs.org/doi/10.1021/jacs.2c05563.

Experimental details of synthesis and spectroscopic measurements; computational details; spectral fitting procedure; and mathematical formula for the simulation of electric field and electric potential (PDF)

■ AUTHOR INFORMATION

Corresponding Authors

Clifford P. Kubiak − *Department of Chemistry and Biochemistry, University of California, San Diego, San Diego, California 92093, United States;* orcid.org/0000-0003-2186-488X; Email: ckubiak@ucsd.edu

Victor S. Batista − *Department of Chemistry and Energy Sciences Institute, Yale University, New Haven, Connecticut 06520, United States;* orcid.org/0000-0002-3262-1237; Email: victor.batista@yale.edu

Tianquan Lian − *Department of Chemistry, Emory University, Atlanta, Georgia 30322, United States;* orcid.org/0000-0002-8351-3690; Email: tlian@emory.edu

Authors

Dhritiman Bhattacharyya − *Department of Chemistry, Emory University, Atlanta, Georgia 30322, United States;* orcid.org/0000-0001-6761-8655

Pablo E. Videla − *Department of Chemistry and Energy Sciences Institute, Yale University, New Haven, Connecticut 06520, United States;* orcid.org/0000-0003-0742-0342

Joseph M. Palasz − *Department of Chemistry and Biochemistry, University of California, San Diego, San Diego, California 92093, United States*

Isaac Tangen − *Department of Chemistry, Emory University, Atlanta, Georgia 30322, United States*

Jinhui Meng − *Department of Chemistry, Emory University, Atlanta, Georgia 30322, United States*

Complete contact information is available at: https://pubs.acs.org/10.1021/jacs.2c05563

Notes

The authors declare no competing financial interest.

■ ACKNOWLEDGMENTS

This work was supported by the AFOSR grant #FA9550-17-0198 (V.S.B., T.L., and C.P.K.), MURI grant FA9550-18-1-0420 (T.L.), and DURIP grant FA9550-18-1-0005 (T. L.). V.S.B. acknowledges high-performance computing time from NERSC, DOD Copper, and from the Yale Center for Research Computing. The authors also want to thank Kyle Angle from the Grassian lab at UCSD for helping them measure the solution Raman spectrum of the sample.

■ REFERENCES

(1) Bhattacharyya, D.; Videla, P. E.; Cattaneo, M.; Batista, V. S.; Lian, T.; Kubiak, C. P. Vibrational Stark shift spectroscopy of catalysts under the influence of electric fields at electrode−solution interfaces. *Chem. Sci.* **2021**, *12*, 10131−10149.

(2) Ge, A.; Rudshteyn, B.; Videla, P. E.; Miller, C. J.; Kubiak, C. P.; Batista, V. S.; Lian, T. Heterogenized Molecular Catalysts: Vibrational Sum-Frequency Spectroscopic, Electrochemical, and Theoretical Investigations. *Acc. Chem. Res.* **2019**, *52*, 1289−1300.

(3) Gorin, C. F.; Beh, E. S.; Bui, Q. M.; Dick, G. R.; Kanan, M. W. Interfacial Electric Field Effects on a Carbene Reaction Catalyzed by Rh Porphyrins. *J. Am. Chem. Soc.* **2013**, *135*, 11257−11265.

(4) Lau, V. M.; Gorin, C. F.; Kanan, M. W. Electrostatic control of regioselectivity via ion pairing in a Au(i)-catalyzed rearrangement. *Chem. Sci.* **2014**, *5*, 4975−4979.

(5) Lau, V. M.; Pfalzgraff, W. C.; Markland, T. E.; Kanan, M. W. Electrostatic Control of Regioselectivity in Au(I)-Catalyzed Hydroarylation. *J. Am. Chem. Soc.* **2017**, *139*, 4035−4041.

(6) Heo, J.; Ahn, H.; Won, J.; Son, J. G.; Shon, H. K.; Lee, T. G.; Han, S. W.; Baik, M.-H. Electro-inductive effect: Electrodes as functional groups with tunable electronic properties. *Science* **2020**, *370*, 214−219.

(7) Vayenas, C. G.; Bebelis, S.; Neophytides, S. Non-Faradaic electrochemical modification of catalytic activity. *J. Phys. Chem. A* **1988**, *92*, 5083−5085.

(8) Meir, R.; Chen, H.; Lai, W.; Shaik, S. Oriented Electric Fields Accelerate Diels−Alder Reactions and Control the endo/exo Selectivity. *ChemPhysChem* **2010**, *11*, 301−310.

(9) Aragonès, A. C.; Haworth, N. L.; Darwish, N.; Ciampi, S.; Bloomfield, N. J.; Wallace, G. G.; Diez-Perez, I.; Coote, M. L. Electrostatic catalysis of a Diels−Alder reaction. *Nature* **2016**, *531*, 88−91.

(10) Shaik, S.; Mandal, D.; Ramanan, R. Oriented electric fields as future smart reagents in chemistry. *Nat. Chem.* **2016**, *8*, 1091−1098.

(11) Cowan, A. J.; Hardwick, L. J. Advanced Spectroelectrochemical Techniques to Study Electrode Interfaces Within Lithium-Ion and Lithium-Oxygen Batteries. *Annual Rev. Anal. Chem.* **2019**, *12*, 323−346.

(12) Gouy, M.On the constitution of the electric charge on the surface of an electrolyte *J. Phys. Theor. Appl.*, 1910; Vol. *9* 1, pp 457−468 DOI: 10.1051/jphystap:019100090045700.

(13) Stern, O. The theory of the electrolytic double-layer. *Z. Elektrochem.* **1924**, *30*, 1014−1020.

(14) Chapman, D. L. LI. A contribution to the theory of electrocapillarity. *London, Edinburgh, Dublin Philosophical Magazine J. Sci.* **1913**, *25*, 475−481.
(15) Bockris, J. M.; Devanathan, M.; Müller, K. On the structure of charged interfaces. *Proc. R. Soc. A* **1963**, *274*, 55−79.
(16) Attard, P. Ion condensation in the electric double layer and the corresponding Poisson-Boltzmann effective surface charge. *J. Phys. Chem. C* **1995**, *99*, 14174−14181.
(17) Andrews, S. S.; Boxer, S. G. Vibrational stark effects of nitriles I. Methods and experimental results. *J. Phys. Chem. A* **2000**, *104*, 11853−11863.
(18) Bublitz, G. U.; Boxer, S. G. Stark spectroscopy: applications in chemistry, biology, and materials science. *Annu. Rev. Phys. Chem.* **1997**, *48*, 213−242.
(19) Fried, S. D.; Boxer, S. G. Measuring Electric Fields and Noncovalent Interactions Using the Vibrational Stark Effect. *Acc. Chem. Res.* **2015**, *48*, 998−1006.
(20) Montenegro, A.; Dutta, C.; Mammetkuliev, M.; Shi, H.; Hou, B.; Bhattacharyya, D.; Zhao, B.; Cronin, S. B.; Benderskii, A. V. Asymmetric response of interfacial water to applied electric fields. *Nature* **2021**, *594*, 62−65.
(21) Lambert, D. K. Vibrational Stark effect of adsorbates at electrochemical interfaces. *Electrochim. Acta* **1996**, *41*, 623−630.
(22) Lambert, D. K. Vibrational Stark effect of CO on Ni (100), and CO in the aqueous double layer: Experiment, theory, and models. *J. Chem. Phys.* **1988**, *89*, 3847−3860.
(23) Bishop, D. M. The vibrational Stark effect. *J. Chem. Phys.* **1993**, *98*, 3179−3184.
(24) Oklejas, V.; Sjostrom, C.; Harris, J. M. SERS detection of the vibrational stark effect from nitrile-terminated SAMs to probe electric fields in the diffuse double-layer. *J. Am. Chem. Soc.* **2002**, *124*, 2408−2409.
(25) Koper, M. T. M.; van Santen, R. A.; Wasileski, S. A.; Weaver, M. J. Field-dependent chemisorption of carbon monoxide and nitric oxide on platinum-group (111) surfaces: Quantum chemical calculations compared with infrared spectroscopy at electrochemical and vacuum-based interfaces. *J. Chem. Phys.* **2000**, *113*, 4392−4407.
(26) Gardner, A. M.; Saeed, K. H.; Cowan, A. J. Vibrational sum-frequency generation spectroscopy of electrode surfaces: studying the mechanisms of sustainable fuel generation and utilisation. *Phys. Chem. Chem. Phys.* **2019**, *21*, 12067−12086.
(27) Neri, G.; Donaldson, P. M.; Cowan, A. J. The role of electrode−catalyst interactions in enabling efficient CO2 reduction with Mo (bpy)(CO) 4 as revealed by vibrational sum-frequency generation spectroscopy. *J. Am. Chem. Soc.* **2017**, *139*, 13791−13797.
(28) Li, J.-F.; Zhang, Y.-J.; Rudnev, A. V.; Anema, J. R.; Li, S.-B.; Hong, W.-J.; Rajapandiyan, P.; Lipkowski, J.; Wandlowski, T.; Tian, Z.-Q. Electrochemical shell-isolated nanoparticle-enhanced Raman spectroscopy: correlating structural information and adsorption processes of pyridine at the Au (hkl) single crystal/solution interface. *J. Am. Chem. Soc.* **2015**, *137*, 2400−2408.
(29) Sarkar, S.; Patrow, J. G.; Voegtle, M. J.; Pennathur, A. K.; Dawlaty, J. M. Electrodes as Polarizing Functional Groups: Correlation between Hammett Parameters and Electrochemical Polarization. *J. Phys. Chem. C* **2019**, *123*, 4926−4937.
(30) Shi, H.; Cai, Z.; Patrow, J.; Zhao, B.; Wang, Y.; Wang, Y.; Benderskii, A.; Dawlaty, J.; Cronin, S. B. Monitoring Local Electric Fields at Electrode Surfaces Using Surface Enhanced Raman Scattering-Based Stark-Shift Spectroscopy during Hydrogen Evolution Reactions. *ACS Appl. Mater. Interfaces* **2018**, *10*, 33678−33683.
(31) Guyot-Sionnest, P.; Tadjeddine, A. Spectroscopic investigations of adsorbates at the metal—electrolyte interface using sum frequency generation. *Chem. Phys. Lett.* **1990**, *172*, 341−345.
(32) Le Rille, A.; Tadjeddine, A. In situ visible-infrared sum and difference frequency generation at the electrochemical interface. *J. Electroanal. Chem.* **1999**, *467*, 238−248.
(33) Tadjeddine, M.; Flament, J.-P.; Le Rille, A.; Tadjeddine, A. SFG experiment and ab initio study of the chemisorption of CN− on low-index platinum surfaces. *Surf. Sci.* **2006**, *600*, 2138−2153.
(34) Rambaud, C.; Cagnon, L.; Levy, J.-P.; Tourillon, G. SFG study of thiocyanate ion adsorption onto polycrystalline Au electrode and electrodeposited metallic thin films. *J. Electrochem. Soc.* **2004**, *151*, No. E352.
(35) Tadjeddine, A.; Le Rille, A. Adsorption of cyanide on gold single crystal investigated by in situ visible−infrared difference frequency generation. *Electrochim. Acta* **1999**, *45*, 601−609.
(36) Wasileski, S. A.; Koper, M. T.; Weaver, M. J. Metal electrode−chemisorbate bonding: General influence of surface bond polarization on field-dependent binding energetics and vibrational frequencies. *J. Chem. Phys.* **2001**, *115*, 8193−8203.
(37) Wasileski, S. A.; Koper, M. T.; Weaver, M. J. Field-dependent electrode− chemisorbate bonding: sensitivity of vibrational Stark effect and binding energetics to nature of surface coordination. *J. Am. Chem. Soc.* **2002**, *124*, 2796−2805.
(38) Weaver, M. J.; Gao, X. In-situ electrochemical surface science. *Annu. Rev. Phys. Chem.* **1993**, *44*, 459−494.
(39) Zou, S.; Weaver, M. J. Potential-Dependent Metal− Adsorbate Stretching Frequencies for Carbon Monoxide on Transition-Metal Electrodes: Chemical Bonding versus Electrostatic Field Effects. *J. Phys. Chem. B* **1996**, *100*, 4237−4242.
(40) Sorenson, S. A.; Patrow, J. G.; Dawlaty, J. M. Solvation Reaction Field at the Interface Measured by Vibrational Sum Frequency Generation Spectroscopy. *J. Am. Chem. Soc.* **2017**, *139*, 2369−2378.
(41) Smith, C. P.; White, H. S. Theory of the interfacial potential distribution and reversible voltammetric response of electrodes coated with electroactive molecular films. *Anal. Chem.* **1992**, *64*, 2398−2405.
(42) Fawcett, W. R. Discreteness-of-charge effects at an electrode covered with a self-assembled monolayer containing a simple redox couple. *J. Electroanal. Chem.* **1994**, *378*, 117−124.
(43) Eggers, P. K.; Darwish, N.; Paddon-Row, M. N.; Gooding, J. J. Surface-bound molecular rulers for probing the electrical double layer. *J. Am. Chem. Soc.* **2012**, *134*, 7539−7544.
(44) Wen, B.-Y.; Lin, J.-S.; Zhang, Y.-J.; Radjenovic, P. M.; Zhang, X.-G.; Tian, Z.-Q.; Li, J.-F. Probing Electric Field Distributions in the Double Layer of a Single-Crystal Electrode with Angstrom Spatial Resolution using Raman Spectroscopy. *J. Am. Chem. Soc.* **2020**, *142*, 11698−11702.
(45) Gruenbaum, S. M.; Henney, M. H.; Kumar, S.; Zou, S. Surface-enhanced Raman spectroscopic study of 1, 4-phenylene diisocyanide adsorbed on gold and platinum-group transition metal electrodes. *J. Phys. Chem. B* **2006**, *110*, 4782−4792.
(46) Ge, A.; Videla, P. E.; Lee, G. L.; Rudshteyn, B.; Song, J.; Kubiak, C. P.; Batista, V. S.; Lian, T. Interfacial Structure and Electric Field Probed by in Situ Electrochemical Vibrational Stark Effect Spectroscopy and Computational Modeling. *J. Phys. Chem. C* **2017**, *121*, 18674−18682.
(47) Clark, M. L.; Grice, K. A.; Moore, C. E.; Rheingold, A. L.; Kubiak, C. P. Electrocatalytic CO 2 reduction by M (bpy-R)(CO) 4 (M= Mo, W; R= H, t Bu) complexes. Electrochemical, spectroscopic, and computational studies and comparison with group 7 catalysts. *Chem. Sci.* **2014**, *5*, 1894−1900.
(48) Cattaneo, M.; Guo, F.; Kelly, H. R.; Videla, P. E.; Kiefer, L.; Gebre, S.; Ge, A.; Liu, Q.; Wu, S.; Lian, T.; Batista, V. S. Robust Binding of Disulfide-Substituted Rhenium Bipyridyl Complexes for CO2 Reduction on Gold Electrodes. *Front. Chem.* **2020**, *8*, 86.
(49) Ge, A.; Rudshteyn, B.; Psciuk, B. T.; Xiao, D.; Song, J.; Anfuso, C. L.; Ricks, A. M.; Batista, V. S.; Lian, T. Surface-Induced Anisotropic Binding of a Rhenium CO2-Reduction Catalyst on Rutile TiO2(110) Surfaces. *J. Phys. Chem. C* **2016**, *120*, 20970−20977.
(50) Grubisha, D. S.; Rommel, J. S.; Lane, T. M.; Tysoe, W. T.; Bennett, D. W. Communication between metal centers in tungsten(0)-tungsten(II) complexes bridged by 1,4-diisocyanobenzene: is the ligand.pi. system involved? *Inorg. Chem.* **1992**, *31*, 5022−5027.
(51) Burdett, J. K.; Downs, A. J.; Gaskill, G. P.; Graham, M. A.; Turner, J. J.; Turner, R. F. Characterization by infrared and Raman

spectroscopy of matrix-isolated M (CO) 5N2 (M= chromium, molybdenum, or tungsten) produced by photolysis of M (CO) 6. *Inorg. Chem.* **1978**, *17*, 523−532.
(52) Bhattacharyya, D.; Montenegro, A.; Plymale, N. T.; Dutta, C.; Lewis, N. S.; Benderskii, A. V. Vibrational Sum Frequency Generation Spectroscopy Measurement of the Rotational Barrier of Methyl Groups on Methyl-Terminated Silicon (111) Surfaces. *J. Phys. Chem. Lett.* **2019**, *10*, 5434−5439.
(53) Robertson, M. J.; Angelici, R. J. Adsorption of aryl and alkyl isocyanides on powdered gold. *Langmuir* **1994**, *10*, 1488−1492.
(54) Henderson, J. I.; Feng, S.; Bein, T.; Kubiak, C. P. Adsorption of diisocyanides on gold. *Langmuir* **2000**, *16*, 6183−6187.
(55) Swanson, S. A.; McClain, R.; Lovejoy, K. S.; Alamdari, N. B.; Hamilton, J. S.; Scott, J. C. Self-assembled diisocyanide monolayer films on gold and palladium. *Langmuir* **2005**, *21*, 5034−5039.
(56) Ito, M.; Noguchi, H.; Ikeda, K.; Uosaki, K. Substrate dependent structure of adsorbed aryl isocyanides studied by sum frequency generation (SFG) spectroscopy. *Phys. Chem. Chem. Phys.* **2010**, *12*, 3156−3163.
(57) Kim, H. S.; Lee, S. J.; Kim, N. H.; Yoon, J. K.; Park, H. K.; Kim, K. Adsorption characteristics of 1, 4-phenylene diisocyanide on gold nanoparticles: infrared and Raman spectroscopy study. *Langmuir* **2003**, *19*, 6701−6710.
(58) Han, H. S.; Han, S. W.; Joo, S. W.; Kim, K. Adsorption of 1, 4-phenylene diisocyanide on silver investigated by infrared and Raman spectroscopy. *Langmuir* **1999**, *15*, 6868−6874.
(59) Bhattacharyya, D.; Dhar, P.; Liu, Y.; Djurovich, P. I.; Thompson, M. E.; Benderskii, A. V. A Vibrational Sum Frequency Generation Study of the Interference Effect in a Thin Film of 4, 4′-Bis (N-Carbazolyl)-1, 10-Biphenyl (CBP) and the Interfacial Orientation. *ACS Appl. Mater. Interfaces* **2020**, *12*, 26515−26524.
(60) Dhar, P.; Plymale, N. T.; Malyk, S.; Lewis, N. S.; Benderskii, A. V. Vibrational Sum-Frequency Spectroscopic Investigation of the Structure and Azimuthal Anisotropy of Propynyl-Terminated Si (111) Surfaces. *J. Phys. Chem. C* **2017**, *121*, 16872−16878.
(61) Park, E. S.; Andrews, S. S.; Hu, R. B.; Boxer, S. G. Vibrational stark spectroscopy in proteins: A probe and calibration for electrostatic fields. *J. Phys. Chem. B* **1999**, *103*, 9813−9817.
(62) Cai, W.-B.; Wan, L.-J.; Noda, H.; Hibino, Y.; Ataka, K.; Osawa, M. Orientational phase transition in a pyridine adlayer on gold (111) in aqueous solution studied by in situ infrared spectroscopy and scanning tunneling microscopy. *Langmuir* **1998**, *14*, 6992−6998.
(63) Kolb, D.; Schneider, J. Surface reconstruction in electrochemistry: Au (100-(5× 20), Au (111)-(1× 23) and Au (110)-(1× 2). *Electrochim. Acta* **1986**, *31*, 929−936.
(64) Stolberg, L.; Morin, S.; Lipkowski, J.; Irish, D. Adsorption of pyridine at the Au (111)-solution interface. *J. Electroanal. Chem. Interfacial Electrochem.* **1991**, *307*, 241−262.
(65) Valette, G. Hydrophilicity of metal surfaces: silver, gold and copper electrodes. *J. Electroanal. Chem. Interfacial Electrochem.* **1982**, *139*, 285−301.
(66) Wright, D.; Sangtarash, S.; Mueller, N. S.; Lin, Q.; Sadeghi, H.; Baumberg, J. J. Vibrational Stark Effects: Ionic Influence on Local Fields. *J. Phys. Chem. Lett.* **2022**, *13*, 4905−4911.
(67) Delley, M. F.; Nichols, E. M.; Mayer, J. M. Interfacial Acid−Base Equilibria and Electric Fields Concurrently Probed by In Situ Surface-Enhanced Infrared Spectroscopy. *J. Am. Chem. Soc.* **2021**, *143*, 10778−10792.
(68) Ge, A.; Kastlunger, G.; Meng, J.; Lindgren, P.; Song, J.; Liu, Q.; Zaslavsky, A.; Lian, T.; Peterson, A. A. On the coupling of electron transfer to proton transfer at electrified interfaces. *J. Am. Chem. Soc.* **2020**, *142*, 11829−11834.
(69) Fu, L.; Wang, Z.; Psciuk, B. T.; Xiao, D.; Batista, V. S.; Yan, E. C. Characterization of parallel β-sheets at interfaces by chiral sum frequency generation spectroscopy. *J. Phys. Chem. Lett.* **2015**, *6*, 1310−1315.
(70) Fu, L.; Xiao, D.; Wang, Z.; Batista, V. S.; Yan, E. C. Chiral sum frequency generation for in situ probing proton exchange in antiparallel β-sheets at interfaces. *J. Am. Chem. Soc.* **2013**, *135*, 3592−3598.

https://doi.org/10.1021/jacs.2c05563
J. Am. Chem. Soc. 2022, 144, 14330−14338